Revista Mexicana de Astronomía y Astrofísica, **51**, 133–145 (2015)

CHEMICAL ABUNDANCES AND PHYSICAL PARAMETERS OF HII REGIONS IN THE MAGELLANIC CLOUDS

R. E. Carlos Reyes,[1,2] F. A. R. Navarro,[1] J. Meléndez,[3] J. Steiner,[3] and F. Elizalde[4]

Received December 23 2014; accepted February 15 2015

RESUMEN

Usamos datos en la región ultravioleta, visible e infrarroja de 11 regiones HII en las Nubes de Magallanes, a fin de determinar sus parámetros físicos y abundancias químicas. Así, hacemos un modelo de fotoionización de seis regiones HII en la Gran Nube de Magallanes (GNM) y cinco regiones HII en la Pequeña Nube de Magallanes (PNM), lo cual nos permite calcular las abundancias de He, C, N, O, Ne, S y Ar. Los valores calculados se comparan con los encontrados en la literatura para regiones HII, nebulosas planetarias y estrellas. Obtuvimos los valores de las abundancias ajustando modelos del código CLOUDY para las intensidades de línea observadas. Además, las observaciones en el Observatório Pico dos Dias de [S II] λ6717/λ6731 para regiones HII en la PNM nos permiten determinar la densidad electrónica. Los datos IUE de las líneas [C III] λ1909 se usan para determinar la abundancia de C de seis y cinco regiones HII en la GNM y en la PNM, respectivamente.

ABSTRACT

We used ultraviolet, optical and infrared data of eleven HII regions in the Magellanic Clouds in order to determine their physical parameters and chemical abundances. The photoionization modeling of six HII regions in the LMC and five HII regions in the SMC, allowed us to derive the abundances of He, C, N, O, Ne, S and Ar, which were compared with those obtained in the literature for HII regions, PN, and stars. The abundances were obtained by adjusting models of the CLOUDY code to the observed line intensities. The observations obtained at the *Observatório Pico dos Dias* of [S II] λ6717/λ6731 line ratios for HII regions in the SMC allowed the determination of the electron density with a high precision. Furthermore, the IUE data on [C III] λ1909 lines were used to determine the abundance of carbon of six and five HII regions in the LMC and SMC, respectively.

Key Words: HII regions — Magellanic Clouds — methods: data analysis

1. INTRODUCTION

The Magellanic Clouds (MCs) are very important for stellar evolution studies, as well as for studies of the chemical evolution of galaxies, because both the small and large Magellanic Clouds (SMC and LMC, respectively) are more metal-poor than the Milky Way. An important motivation for determining the chemical abundances in low metallicity systems is related to the determination of the primordial helium abundance, which is a fundamental constraint to the Big Bang theory (Peimbert et al. 2007; Olive & Steigman 1995; Peimbert & Torres-Peimbert 1974, 1976; Kajino et al. 2012; Smecker-Hane et al. 2002; Steigman 2004). There are several previous studies concerning the chemical abundances of MCs HII regions (e.g., Vermeij and van der Hulst 2002); however, most of them are based on few (or only one) HII regions or use only ICF's. Besides, not all of them use the same methods, so it is difficult to compare different results.

Regarding stellar evolution, a study of CNO elements is of particular interest because they are involved in a variety of processes, wherein these ele-

[1]Universidad Nacional Mayor de San Marcos, UNMSM, Lima, Peru.
[2]Universidad Nacional del Callao, UNAC, Callao, Peru.
[3]Universidade de São Paulo, IAG/USP, São Paulo, Brazil.
[4]Instituto Nacional de Pesquisas Espaciais, Divisão de Astrofísica - DAS/INPE, São Paulo, Brazil.

ments are either synthesized or destroyed. Carbon is produced by massive stars (M > $10M_{\odot}$) and intermediate mass stars (Peters et al. 2010); nitrogen is produced only by the latter and it is considered a secondary element (Mowlavi 2001); oxygen is synthesized almost exclusively by massive stars; this element is an important tracer of type-II supernovae (SNII) (Stasińska 2012; Garnett et al. 1995). Stellar winds during the asymptotic giant branch (AGB) can enrich the interstellar medium (ISM) with C and N, while the C/N ratio is related to the convective mixing in the stellar interiors. The abundances of C/H and N/H show a time delay with respect to oxygen; their values can, in principle, serve as a potential *clock* to determine the relative ages of stellar systems (Pettini 2004; Garnett et al. 1995). Heavier elements such as neon, sulfur and argon are easily observed in ionized nebulae from ground-based telescopes; as these elements do not participate in the CNO cycle, being produced mainly by type II supernovae, their analysis becomes interesting when they are compared to the CNO cycle.

Furthermore, a detailed photoionization modelling, as the one that will be presented here, offers the opportunity to identify, in a self-consistent way, other important parameters such as luminosity, ionization temperature, dust/gas ratio, total ionized mass, filling factor, optical depth, etc. Studies of these physical parameters not only have impact on the star formation theory but also are related to the chemical abundances. For example, part of C and O may be in the form of dust grains, or the dust/gas may be directly related to the carbon abundance (Mathis 1990).

It is well established that abundances of elements such as CNO in MCs are significantly lower than the corresponding solar abundances; they are also lower than the abundances observed in nebulae in our galaxy (Peimbert et al. 1993; Leisy & Dennefeld 2006). Other anomalies such as either carbon deficiency in the SMC (Dufour 1984; Rolleston et al. 2003) or absence of the UV bump in the SMC (Rocca et al. 1981; Sofia et al. 2006) have been clearly established. In the SMC, the primary-element abundances are deficient by a factor of 6 when compared to the equivalent solar abundances; whereas in the LMC the factor is 3 (Dufour et al. 1982). Concerning the secondary elements, for nitrogen the ratios are 23 and 11, respectively; the helium abundances are apparently smaller in HII regions of the MCs than in HII regions of nearby spiral galaxies. These results have stimulated observational studies of HII regions in other galaxies.

TABLE 1

EQUATORIAL COORDINATES FOR THE HII REGIONS

Object	R.A. 1950			Dec. 1950		
	(h)	(m)	(s)	(°)	(′)	(″)
LMC:						
N4A	04	52	05.3	-67	00	12
N11A	04	57	09.7	-66	27	52
N79A	04	52	07.9	-69	28	35
N157	05	39	06.7	-69	06	40
N159	05	40	31.1	-69	46	06
N160	05	40	09.3	-69	40	18
SMC:						
N12B	00	43	39.9	-73	21	14
N66	00	57	28.0	-72	26	08
N81	01	07	48.0	-73	28	00
N83A	01	12	23.4	-73	33	52
N88	01	22	54.8	-73	24	52

In this paper, we present the results of detailed photoionization models involving spectroscopic data in the optical and UV bands of eleven HII regions in the MCs, and also results from IRAS satellite observations in four infrared bands(12, 25, 60 and 100 μm).

2. LITERATURE DATA

The sample consists of 11 HII regions whose coordinates are given in Table 1. Most of our data were obtained from the literature; however, optical observations were made, as described in the next section. Table 2 displays the angular sizes and radii of the HII regions.

2.1. *Ultraviolet*

The ultraviolet spectra (UV) were obtained by using the IUE database; then, they were reprocessed with the last version of the NEWSIPS program, giving slightly larger fluxes than the previous program (IUESIPS, Garhart & Nichols 1995). The IUE image numbers are given in Table 3; the Hβ fluxes reported from ground-based observations were scaled to the UV data by the ratio of the areas of the IUE aperture to the ground-based apertures (Dufour et al. 1982) in all cases except for SMC N81, since due to its small size the object fitted entirely inside both apertures.

TABLE 2

ANGULAR SIZES AND RADII OF THE HII REGIONS

	DEM[a]	Other	D(′)	r (pc)	Source
LMC:					
N4A	8b	NGC1714	1.4	10	a
N11A	—	—	0.2	1.5	b
N79AB	9	IC2111	5.0	36	a
N157AB	263	—	29.2	212	a
N159A-K	271	NGC2079	5.0	36	a
N160A-E	284	NGC2080	12.2	89	a
SMC:					
N12B	15,18	NGC249	2.3	20	a
N66A,B,C,D	103	NGC346	11.9	104	a
N81	138	IC1644	5.3	46	a
N83A,C	147	NGC456	3.3	29	a
N88	161	—	1.8	16	a

[a] Davies et al. (1976), [b] (Heydari-Malayeri & Testor 1985).

2.2. *Optical*

The optical spectroscopic data were taken from several sources: (Dufour & Harlow 1977) (SMC: N12B, N66NW, N81, N88), (Peimbert & Torres-Peimbert 1976), (SMC: N66A), (Dufour et al. 1975) (SMC: N83A), (Peimbert & Torres-Peimbert 1974) (LMC: N4A, N157, N159), (Heydari-Malayeri & Testor 1986) (LMC: N11A) and (Dufour et al. 1975) (LMC: N160A). The Hβ fluxes taken from the literature are given in Table 4, where, additionally, the integrated Hβ fluxes, $F(\mathrm{H}_\beta)_{\mathrm{total}}$, and their respective references are shown. In the table, $\mathrm{A}_{\mathrm{Tel.}}$ stands for the area of the telescope mirror in square arcseconds. The $F(\mathrm{H}_\beta)_{\mathrm{total}}$ values for each HII region of the SMC are taken from (Caplan et al. 1996) with the exception of N66A and N66NW; for the latter object we assumed 0.75 of the flux of DEM103 from (Kennicutt & Hodge 1986), according to the calibration of (Caplan et al. 1996). For the LMC, by using the observed Hα/Hβ ratio, we derived the Hβ fluxes from the Hα fluxes by (Kennicutt & Hodge 1986). The N11A total flux was obtained from the relation between the size of the spectral aperture and the radius of this object, according to (Heydari-Malayeri & Testor 1985).

TABLE 3

IUE OBSERVATIONS

HII	IUE Image	R.A. 1950 (h)	(m)	(s)	Dec. 1950 (°)	(′)	(″)
LMC:							
N4A	27823	04	52	05.3	-67	00	12
N11A	26393	04	57	09.7	-66	27	52
N79A	06979	04	52	07.9	-69	28	35
N157	22110	05	39	06.7	-69	06	40
N159	26356	05	40	31.1	-69	46	06
N160	26382	05	40	09.3	-69	40	18
SMC:							
N12B	33805	00	43	39.9	-73	21	14
N66	07004	00	57	28.0	-72	26	08
N66	44455	00	57	22.8	-72	26	46
N81	08944	01	07	48.0	-73	28	00
N83A	18195	01	12	23.4	-73	33	52
N88	23615	01	22	54.8	-73	24	52

2.3. *Infrared*

The infrared data were taken from IRAS observations, (Schwering & Israel 1990); in Table 5, the IRAS numbers of the sample are given; the N4A IRAS data also include DEM 8a (N4F in Henize 1956). In the case of N79A, the IRAS coordinates are basically the same as the ones from the IUE, but the identification of (Schwering & Israel 1990) corresponds to DEM 10a; the largest difference is 14 arc seconds in declination. For N157 we did not find an IRAS observation with coordinates matching those from the IUE. Therefore, we did not use it. For N66, the IRAS datum corresponds only to the south west of the HII region, whose coordinates agree with those from the IUE; the flux, therefore, should be regarded as a lower limit.

Table 6 shows the fluxes observed by the IRAS satellite as well as the integrated IR flux and the temperature, which were obtained following (Pottasch 1984), that is, adjusting a black-body curve to the IRAS data. The temperatures are very low, possibly because the data are not well fitted by the black-body approximation. Hence, both temperatures and fluxes should be regarded as lower limits. As a first approach, the IR-emitting region and the Hβ region are supposed to be the same, and they will be used in the photoionization code to estimate the dust/gas ratio.

TABLE 4

DATA SOURCE FOR Hβ FLUXES

LMC:						
HII	N4A	N11A	N79A	N157	N159	N160A
log$F$(H$_\beta$)	-11.17	-11.77	-11.24	-10.70	-11.46	-10.75
Ref.	1	6	1	1	1	2, 5
HII	N4A	N11A	N79A,B	N157A,B	N159A−K	N160A−E
log$F$(H$_\beta$)$_{\rm tot.}$	-10.82	-10.97	-9.73	-8.36	-9.75	-9.19
Ref.	7	6	7	7	7	7
log$F$(H$_\beta$)$_{IUE}$	-11.44	-11.97	-11.51	-10.90	-11.73	-11.44
log$F$[CIII]λ1909	-12.33	-12.39	-12.32	-12.03	-12.47	-12.24
A$_{\rm Tel.}(''$)^2	404	16	404	343	404	1035
SMC:						
HII	N12B	N66A	N66NW	N81	N83A	N88
log$F$(H$_\beta$)	-11.81	-11.58	-11.19	-11.06	-11.40	-11.45
Ref.	4	3	4	4	2, 3	4
HII	N12B	N66	N66	N81	N83	N88
log$F$(H$_\beta$)$_{\rm tot.}$	-10.69	-9.41	-9.41	-10.73	-10.43	-10.96
Ref.	8	7, 8	7, 8	8	8	8
log$F$(H$_\beta$)$_{IUE}$	-12.37	-11.85	-11.75	-11.06	-11.40	-11.45
log$F$[CIII]λ1909	-12.88	-12.57	-12.41	-11.64	-12.27	-12.01
A$_{\rm Tel.}(''$)^2	783	404	783	783	1035	783

[1] (Peimbert & Torres-Peimbert 1974), [2] (Dufour et al. 1975), [3] (Peimbert & Torres-Peimbert 1976), [4] (Dufour & Harlow 1977), [5] Caplan & Deharveng (1985), [6] (Heydari-Malayeri & Testor 1985), [7] (Kennicutt & Hodge 1986), [8] (Caplan et al. 1996).

TABLE 5

IRAS OBSERVATIONS

HII Regions	IRAS Number	R. A. 1950 (h)	(m)	(s)	Dec. 1950 (°)	(′)	(″)
LMC:							
N4A	102	04	52	04.8	-67	00	09
N79A	103	04	52	09.5	-69	28	21
N159A-K	1518	05	40	33.3	-69	46	10
N160A-E	1503	05	40	09.0	-69	40	13
SMC:							
N12B	30	00	43	37.1	-73	21	32
N66A,B,C,D	131	00	57	26.5	-72	26	36
N81	187	01	07	43.9	-73	27	40
N88	215	01	22	52.8	-73	24	45

3. OBSERVED OPTICAL DATA

The literature data were complemented with observed optical spectra obtained at the *Observatório Pico dos Dias* (OPD), which is located in Brasopolis, Minas Gerais, southeastern Brazil. These last data were collected in two nights, July 30 and 31, 1997, by using the Boller & Chivens spectrograph, equipped with a CCD camera (Wright Instruments, CCD 048), which is large enough to allow simultaneous observations of object and sky, allowing a subsequent application of the sky-subtraction technique. The slit size was 800 μm (12.5″) by 15000 μm (230″); we use a 900-lines/mm dispersion grating, yielding a spectral resolution about 4 Å, and covering the spectrum from 5540 Å to 6860 Å.

An important application of the OPD observations is the determination of the [S II] line intensities, which are important to determine the gas density in five HII regions. The observation log is presented in Table 7, where the object name, date, observed spectral region, number of images obtained, and in-

TABLE 6

IRAS FLUXES

	Observed Flux (Jy)				$T_{\rm dust}$	log $\mathcal{F}^{\rm IR}_{\rm total}$
	12 μm	25 μm	60 μm	100 μm	(K)	(erg.s^{-1}.cm^{-2})
LMC:						
N4A	3.63	13.99	116.7	191.4	49	-8.07
N79A	9.10	65.16	343.6	353.6	325	-6.94
N159	4.07	33.30	414.0	624.0	51	-7.54
N160	14.98	111.00	662.4	769.6	62	-7.36
SMC:						
N12B	0.22	0.89	14.0	27.0	45	-8.94
N66A	5.99	43.50	200.0	242.0	61	-7.88
N81	0.44	2.55	18.0	27.0	51	-8.90
N88	2.21	22.90	55.0	46.0	94	-8.29

TABLE 7

LOG OF OPTICAL OBSERVATIONS FOR SMC

Object	Date	Spectral Region (ΔÅ)	Number of Images	Integration Time (s)
N12B	July 30, 1997	5540–6860	3	300, 480
N66	July 30, 1997	5540–6860	2	300, 480
N81	July 30, 1997	5540–6860	2	300, 480
N83A	July 31, 1997	5540–6860	4	300, 480
N88	July 31, 1997	5540–6860	3	300, 480

tegration times are given. The data were reduced using the IRAF package in a standard way, namely variations of pixel to pixel sensitivity were corrected with flat-field exposures, and subtraction of bias and dark was carried out. Next, the two-dimensional image was reduced to one-dimension (spectrum extraction), and the calibration was performed on wavelength and flux. Moreover, the response curve of the system was determined through observations of the standard stars LTT7379 and EG21 (Hamuy et al. 1992, 1994), and a curve of average atmospheric extinction was adopted for the OPD, (Jablonski 1996).

For each object, Table 8 lists the observed fluxes of the main nebular lines for N12B, N66, N81, N83A and N88, relative to $F(\mathrm{H}\alpha)$=100. In addition, the approximate wavelength (Å) for each line is shown, as well as the identification of the corresponding ions that produce the respective line. The observed spectra of the objects just mentioned are shown, respectively, in Figures 1, 2, 3, 4 and 5.

TABLE 8

LINE INTENSITIES RELATIVE TO Hα FOR SMC

Ion	λ	N12B	N66	N81	N83A	N88
He I	5876	3.94	3.90	4.32	2.25	—
Hα	6563	100.	100.	100.	100.	100.
[N II]	6584	2.63	2.18	3.32	2.93	3.47
He I	6678	1.51	1.27	1.65	1.03	—
[S II]	6717	3.58	2.69	3.73	3.33	6.16
[S II]	6731	2.93	2.34	3.16	2.64	4.56

4. MODELLING OF THE HII REGIONS

In order to obtain a photoionization model (Osterbrock & Ferland 2005) that best fits different observables of a particular object, we use DIANA, (Elizalde 1997; Carlos-Reyes 1997), an automatic and self-consistent method, which simultaneously

TABLE 9

LINE INTENSITIES OBSERVED AND CALCULATED FOR HII REGIONS OF THE MCS

LMC:														
			N4A		N11A		N79A		N157		N159		N160A	
Ion	λ	f(λ)	obj.	mod.	obj.	mod.	obj.	mod.	obj.	mod.	obj.	mod.	obj.	mod.
[C III]	1909	1.487	0.131	0.131	0.180	0.180	0.157	0.157	0.101	0.101	0.185	0.185	0.159	0.159
[O II]	3727	0.321	1.137	1.246	0.754	0.634	1.790	2.009	0.657	0.830	1.235	1.237	1.030	1.192
[Ne III]	3869	0.277	0.224	0.226	0.263	0.265	0.171	0.171	0.286	0.286	0.264	0.264	0.170	0.170
[S II]	4074	0.219	0.005	0.009	0.000	0.005	0.000	0.023	0.013	0.008	0.000	0.014	0.000	0.013
Hδ	4102	0.212	0.000	0.236	0.230	0.240	0.000	0.225	0.000	0.214	0.000	0.212	0.199	0.248
Hγ	4340	0.152	0.435	0.437	0.424	0.441	0.434	0.421	0.424	0.410	0.412	0.404	0.428	0.451
[O III]	4363	0.054	0.019	0.019	0.023	0.019	0.019	0.021	0.033	0.036	0.028	0.029	0.019	0.022
Hβ	4861	0.000	1.000	1.000	1.000	1.000	1.000	1.000	1.000	1.000	1.000	1.000	1.000	1.000
[O III]	4959	-0.074	1.414	1.380	1.703	1.433	1.350	1.520	1.706	1.877	1.427	1.489	1.540	1.783
He I	5876	-0.275	0.130	0.130	0.139	0.139	0.127	0.127	0.138	0.138	0.142	0.142	0.148	0.148
[S III]	6312	-0.315	0.014	0.028	0.009	0.030	0.000	0.020	0.018	0.044	0.000	0.032	0.022	0.021
Hα	6563	-0.290	3.412	3.415	3.326	3.353	3.682	3.662	3.914	3.891	3.997	3.980	3.060	3.201
[N II]	6584	-0.333	0.153	0.153	0.068	0.068	0.281	0.281	0.116	0.116	0.206	0.206	0.177	0.177
[S II]	6716	-0.335	0.096	0.091	0.034	0.033	0.152	0.152	0.074	0.072	0.175	0.175	0.108	0.108
[S II]	6731	-0.385	0.081	0.077	0.036	0.035	0.171	0.171	0.071	0.069	0.132	0.132	0.091	0.091
[Ar III]	7135	-0.407	0.135	0.135	0.000	0.105	0.157	0.157	0.169	0.169	0.177	0.177	0.208	0.208
[O II]	7325	-0.595	0.049	0.036	0.000	0.024	0.082	0.113	0.032	0.052	0.101	0.059	0.160	0.033
$F_{\rm IR}$	0	-1.000	000.0	90.4	000.0	165.2	000.0	38.2	000.0	111.5	162.4	162.8	000.0	15.4
SMC:														
			N12B		N66A		N66NW		N81		N83A		N88	
Ion	λ	f(λ)	obj.	mod.	obj.	mod.	obj.	mod.	obj.	mod.	obj.	mod.	obj.	mod.
[C III]	1909	1.802	0.307	0.307	0.194	0.194	0.220	0.220	0.259	0.261	0.133	0.133	0.276	0.276
[O II]	3727	0.323	1.493	1.433	0.854	0.980	1.029	1.644	1.245	1.417	1.730	1.726	1.201	1.576
[Ne III]	3869	0.278	0.348	0.348	0.407	0.406	0.336	0.335	0.371	0.372	0.143	0.141	0.317	0.317
Hδ	4102	0.213	0.000	0.240	0.000	0.243	0.000	0.253	0.000	0.255	0.199	0.244	0.000	0.207
Hγ	4340	0.152	0.433	0.443	0.446	0.447	0.460	0.460	0.454	0.463	0.428	0.447	0.411	0.398
[O III]	4363	0.147	0.075	0.070	0.068	0.078	0.060	0.062	0.063	0.072	0.036	0.036	0.085	0.081
Hβ	4861	0.000	1.000	1.000	1.000	1.000	1.000	1.000	1.000	1.000	1.000	1.000	1.000	1.000
[O III]	4959	-0.026	1.685	1.707	1.732	1.788	1.726	1.569	1.773	2.015	1.210	1.206	1.889	1.808
He I	5876	-0.223	0.102	0.101	0.111	0.111	0.114	0.114	0.121	0.121	0.128	0.128	0.127	0.127
[S III]	6312	-0.294	0.000	0.031	0.029	0.027	0.019	0.023	0.020	0.019	0.000	0.037	0.000	0.012
Hα	6563	-0.331	3.281	3.300	3.210	3.211	3.017	3.018	2.949	2.966	3.060	3.241	4.317	4.289
[N II]	6584	-0.334	0.072	0.072	0.050	0.050	0.068	0.068	0.065	0.065	0.102	0.102	0.092	0.092
[S II]	6716	-0.351	0.157	0.156	0.064	0.065	0.081	0.076	0.064	0.053	0.212	0.207	0.108	0.108
[S II]	6731	-0.353	0.129	0.128	0.056	0.057	0.071	0.067	0.053	0.044	0.165	0.163	0.080	0.080
[Ar III]	7135	-0.404	0.000	0.130	0.115	0.115	0.000	0.107	0.070	0.070	0.104	0.104	0.000	0.178
[O II]	7325	-0.426	0.000	0.067	0.027	0.050	0.000	0.069	0.052	0.049	0.000	0.062	0.000	0.105
$F_{\rm IR}$	0	-1.000	56.1	56.1	33.6	33.6	33.6	33.6	68.0	68.0	00.0	14.2	473.4	472.5

obtains the physical conditions and chemical abundances of the nebula, as well as the main characteristics of the ionizing source – DIANA is a Portuguese acronym for Automatic Diagnosis of Astrophysical Nebulae. For collisionally excited lines observed in HII regions, DIANA uses indexes defined by

$$T(\alpha) = a\,\mathbf{log}\left[\, n\,\frac{\sum_i f_i^{\alpha}(EP_i)}{\sum_i f_i^{\alpha}\sum_i(EP_i)}\right], \qquad (1)$$

$$I(\alpha) = b\,\mathbf{log}\left[\, n\,\frac{\sum_i f_i^{\alpha}(IP_i)^{1/2}}{\sum_i f_i^{\alpha}\sum_i(IP_i)^{1/2}}\right], \quad \text{and} \quad (2)$$

$$N(\alpha) = c\,\mathbf{log}\left[\, n\,\frac{\sum_i f_i^{\alpha}\log(Nc_i)}{\sum_i f_i^{\alpha}\sum_i\log(Nc_i)}\right], \qquad (3)$$

where $T(\alpha)$, $I(\alpha)$ and $N(\alpha)$ are, respectively, the indexes of temperature, ionization, and density, which depend on the power α from the line flux f_i^{α}; n is the number of forbidden lines considered; EP_i, IP_i and Nc_i are, respectively, the excitation and ionization potentials, and critical density of the line i; a, b and c are normalization constants. For the spectrum lines produced by recombination, we define

$$I_r = \mathbf{log}\left[n\,\frac{\sum_i f_i(IP_i)^{1/2}}{\sum_i f_i\sum_i(IP_i)^{1/2}}\right], \qquad (4)$$

where f_i stands for the i-th line flux. The total sum of the flux observed in all lines is defined as follows:

$$S = \sum_i f_i.$$

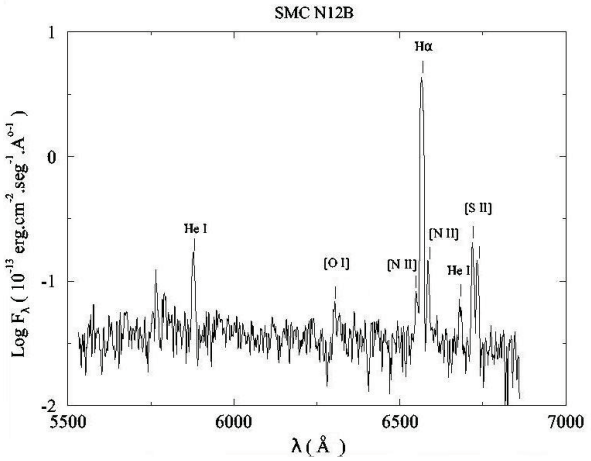

Fig. 1. Observed spectrum for the HII region N12B in the SMC. The emission lines are identified.

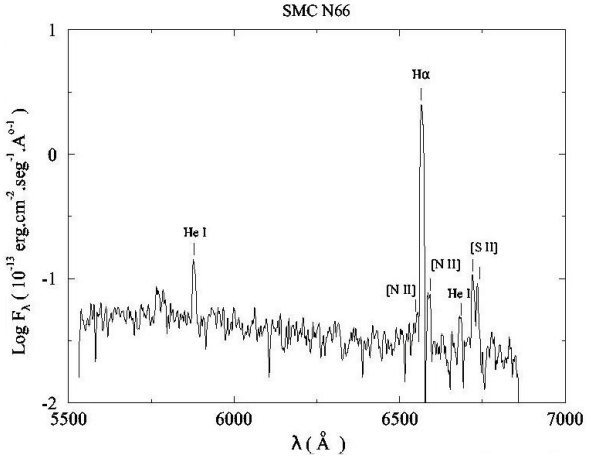

Fig. 2. Observed spectrum for the HII region N66 in the SMC. The emission lines are identified.

Next, the quality parameters are defined. The first one is the Q parameter, which is related to the physical conditions of the system, i.e. Q quantifies the Δ differences between the indexes T, I, N, S and I_r obtained for the model and the observed spectra:

$$Q = \left\{ \Delta T^2 + \Delta I^2 + \Delta N^2 + \Delta S^2 + \Delta I_r^2 \right\}^{1/2} . \quad (5)$$

The second parameter of quality is related to the chemical abundances:

$$R(\alpha) = \frac{\sum_i \left| \frac{f_i^{\rm obs.} - f_i^{\rm cal.}}{f_i^{\rm obs.}} \right| (f_i^{\rm obs.})^\alpha}{\sum_i (f_i^{\rm obs.})^\alpha} \quad , \quad (6)$$

where $f_i^{\rm obs.}$ and $f_i^{\rm cal.}$ are the fluxes observed and calculated for the i-th line. Finally, the third parameter

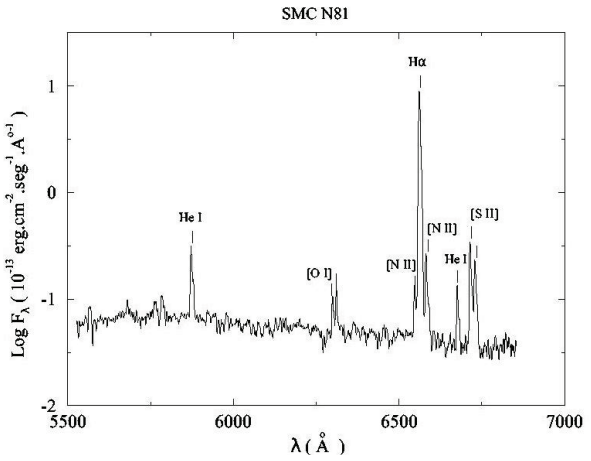

Fig. 3. Observed spectrum for the HII region N81 in the SMC. The emission lines are identified.

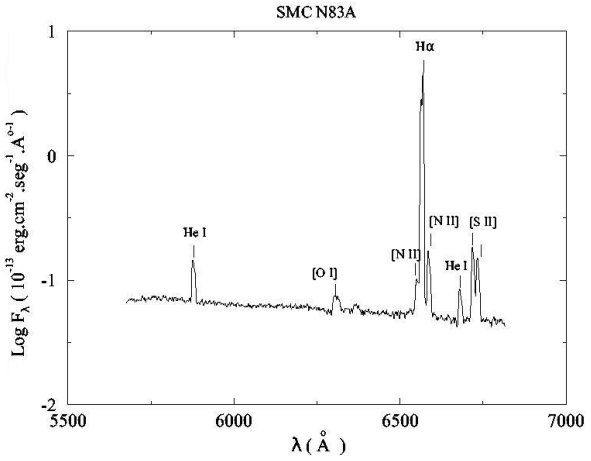

Fig. 4. Observed spectrum for the HII region N83A in the SMC. The emission lines are identified.

H is a quality indicator of the fit for the oxygen line ratios $R1$, $R2$ and $R3$:

$$H = \frac{\left[H' + 3 | I_r^{\rm obs.} - I_r^{\rm cal.} | \right]}{4} \quad , \quad (7)$$

where

$$H' = \frac{2I_{4959}^{\rm obs.} \left| R1^{\rm cal.}/R1^{\rm obs.} - 1 \right| + I_{7325}^{\rm obs.} \left| R2^{\rm cal.}/R2^{\rm obs.} - 1 \right|}{2I_{4959}^{\rm obs.} + I_{7325}^{\rm obs.} + I_{3727}^{\rm obs.}}$$

$$+ \frac{I_{3727}^{\rm obs.} \left| R3^{\rm cal.}/R3^{\rm obs.} - 1 \right|}{2I_{4959}^{\rm obs.} + I_{7325}^{\rm obs.} + I_{3727}^{\rm obs.}} . \quad (8)$$

Specifically, we have $R1 = I(\lambda 4363)/I(\lambda 4959)$; $R2 = I(\lambda 3727)/I(\lambda 7325)$ and $R3 = I(\lambda 3727)/I(\lambda 4959)$.

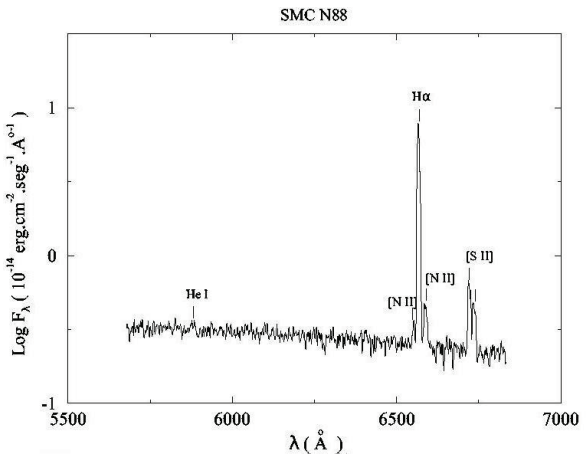

Fig. 5. Observed spectrum for the HII region N88 in the SMC. The emission lines are identified.

DIANA uses the code CLOUDY (Ferland 2004), combined with a Powell minimization routine. (Press et al. 2007). The function to be minimized is $Y = Q + aR + bH$, where Q is defined as a function sensitive to the physical conditions; a and b are constants; R is the weighted relative residual of observed lines intensities (sensitive to chemical abundances), and H is the weighted relative residual of the oxygen and helium line ratios. This last parameter is sensitive to the electron temperature, the electron density and the effective temperature of the ionizing source.

The model assumes spherical symmetry and a density of hydrogen variable throughout the nebula, with a power law $n = n_0 r^\gamma$, where n_0 is the initial density and r the radius of the nebula. The final density n and the γ parameter are fitted using as boundary condition the ratio of sulphur lines intensities $\lambda 6717/\lambda 6731$; if the sulphur lines were not observed, the oxygen line ratio $\lambda 3726/\lambda$ 3729 could be used. The gas temperature is obtained in a self-consistent way by fitting the oxygen line ratio $\lambda 4959/\lambda 4363$.

The functions Q, R and H are calculated for the model spectrum by using internal and interstellar reddening for the nebula.

5. RESULTS

In Table 9 we show the line intensities observed and calculated for HII regions of the MCs. The first and second columns show the ion and the wavelength, respectively; the third column shows the function of (Pei 1992) for reddening correction; and the next paired columns list the names of the objects with their respective lines intensities, observed and modeled. The last row shows the integrated in-

TABLE 10

COMPARISON WITH THE LITERATURE FOR THE MCS

Object	ϵ(He)	ϵ(C)	ϵ(N)	ϵ(O)	ϵ(Ne)	ϵ(S)	ϵ(Ar)	Source
LMC:								
N4A	10.90	—	7.05	8.42	7.51	6.78	6.18	HL
N4A	10.90	—	7.20	8.18	7.56	7.00	6.17	RD
N4A	10.92	8.15	7.43	8.39	7.82	6.91	6.06	TW
N11A	10.92	—	6.85	8.43	7.56	7.19	—	HT
N11A	10.95	8.26	7.45	8.36	7.97	6.96	—	TW
N79A	10.90	—	7.19	8.70	7.93	—	—	PT
N79A	10.90	8.06	7.06	8.49	7.67	7.14	6.15	D
N79A	10.89	8.36	7.19	8.48	7.58	6.72	6.07	TW
N157	10.93	—	7.13	8.55	7.88	—	—	PT
N157	10.95	7.69	6.92	8.27	7.61	6.89	6.09	D
N157	6.78	8.30	7.84	6.77	6.21			M
N157	7.82	8.30						G
N157	10.92	7.87	7.31	8.27	7.61	6.82	5.96	TW
N159A	10.97	—	6.96	8.40	7.56	7.27	—	HT
N159A	10.95	—	6.91	8.21	7.44	—	—	PT
N159A	10.86	—	6.87	8.39	—	—	—	P
N159A	—	—	7.21	8.45	7.56	6.80	—	A
N159A	10.93	7.79	6.84	8.27	7.64	7.03	6.02	D
N159A	10.93	8.18	7.05	8.20	7.50	6.67	5.97	TW
N160A1	10.93	—	6.91	8.44	7.80	6.68	—	HT86
N160A2	10.90	—	6.82	8.33	7.65	6.57	—	HT86
N160A3	10.90	—	6.89	8.36	7.74	6.60	—	HT86
N160A	10.96	—	7.07	8.44	7.62	6.80	—	D75
N160A	—	—	7.03	8.45	7.68	6.76	—	A
N160A	10.99	8.21	7.39	8.50	7.48	6.90	6.35	TW
SMC:								
N12B	10.87	—	6.36	7.95	7.24	6.43	—	DH
N12B	10.88	7.45	6.51	7.97	7.17	6.42	—	TW
N66	10.90	7.12	6.45	7.98	7.35	6.63	5.83	D
N66	10.92	7.17	6.66	8.06	7.33	6.59	—	DH
N66	10.91	7.11	6.55	7.91	7.20	6.30	5.68	TW
N66	10.92	7.17	6.57	7.97	7.23	6.32	—	TW
N81	10.93	7.18	6.65	8.09	7.35	6.44	5.71	D
N81	10.94	—	6.33	7.90	7.17	6.05	5.88	H88
N81	10.93	—	6.49	8.07	7.37	6.26	—	DH
N81	10.97	7.30	6.75	8.09	7.29	6.32	5.59	TW
N83A	11.00	—	6.46	8.05	7.15	—	6.76	D75
N83A	10.95	7.39	6.65	8.03	7.06	6.66	5.75	TW
N88A-b	—	7.40	6.60	8.09	—	—	—	K
N88A-s	—	7.51	6.68	8.11	—	—	—	K
N88A	10.89	—	—	8.04	7.34	6.54	—	TP
N88	10.89	—	—	7.91	7.21	6.08	—	DH
N88	—	7.37	—	8.09	—	—	—	G
N88	10.90	7.79	6.30	7.95	7.10	5.89	—	TW

References: (Heydari-Malayeri & Testor 1985)(HT); (Peimbert & Torres-Peimbert 1974)(PT); (Heydari-Malayeri & Lecavelier des Etangs 1994)(HL); (Dufour et al. 1982)(D); (Aller et al. 1979)(A); (Russell & Dopita 1990)(RD); (Heydari-Malayeri & Testor 1986)(HT86); (Dufour et al. 1975)(D75); (Garnett et al. 1995)(G); (Pagel et al. 1978)(P); (Mathis et al. 1985)(M); (Dufour & Harlow 1977)(DH); (Heydari-Malayeri et al. 1988)(H88); (Kurt et al. 1995)(K); (Testor & Pakull 1985)(TP); This work (TW).

TABLE 11

CHEMICAL ABUNDANCES,
ϵ=LOG(X/H) + 12

HII	ϵ(He)	ϵ(C)	ϵ(N)	ϵ(O)	ϵ(Ne)	ϵ(S)	ϵ(Ar)	ϵ(Z)
LMC:								
N4A	10.92	8.15	7.43	8.39	7.82	6.91	6.06	6.93
N11A	10.95	8.26	7.45	8.36	7.97	6.96	—	6.97
N79A	10.89	8.36	7.19	8.48	7.58	6.72	6.07	6.79
N157	10.92	7.87	7.31	8.27	7.61	6.82	5.96	6.80
N159	10.93	8.18	7.05	8.20	7.50	6.67	5.97	6.71
N160A	10.99	8.21	7.39	8.50	7.48	6.90	6.35	6.91
Median	10.93	8.03	7.37	8.33	7.73	6.82	5.97	6.85
SMC:								
N12B	10.88	7.45	6.51	7.97	7.17	6.42	—	6.44
N66A	10.91	7.11	6.55	7.91	7.20	6.30	5.68	6.39
N66NW	10.92	7.17	6.57	7.97	7.23	6.32	—	6.42
N81	10.97	7.30	6.75	8.09	7.29	6.32	5.59	6.40
N83A	10.95	7.39	6.65	8.03	7.06	6.66	5.75	6.49
N88	10.90	7.79	6.30	7.95	7.10	5.89	—	6.25
Median	10.91	7.39	6.55	7.96	7.17	6.32	5.72	6.43

frared flux obtained from IRAS data. For comparison, we also show in Table 10 our results for each object along with the literature values. The object name is given in the first column. Colums 2 to 8 list the chemical abundances; in the last column we display the references. In general we observe agreement between our results and those from the literature.

In Table 11 we present again the chemical abundances obtained from the model; specifically, for the HII regions indicated in the first colum. Columns 2 to 9 show, respectively, the logarithm of the chemical abundances (element X relative to hydrogen, $\log[X/H]+12$) of helium, carbon, nitrogen, oxygen, neon, sulphur and argon. In the last column, Z provides the geometric mean of the abundances of neon, sulphur and argon; this value will be used as an indicator of the nebular metallicity. Based on the intensity of the lines and on the number of ionization states, we estimate the error for the respective abundances as follows: 0.03 dex for helium, nitrogen and oxygen; 0.06 dex for carbon and neon; and 0.08 dex for sulphur and argon. In Table 12, we compare the average chemical abundances, obtained by us with literature results for the LMC and SMC, of FGK stars, B stars and planetary nebulae (PN). For the Milky Way we compare our results with the Sun, the Orion nebula and the Galactic HII regions M8 and M17. In addition, in Table 13 we show a comparison between the average of our results and those from the literature.

In Table 10 we also see that the carbon abundance is higher than those found by (Dufour et al. 1982); in part this is due to a different extinction curve used. They used the UV results of (Seaton 1979), which were derived from a study of the PN NGC 7027. For the carbon abundance determination the major uncertainties are due to the different positions observed between the IUE satellite and ground-based telescopes. This is supported by studies of (Heydari-Malayeri & Testor 1982, 1985, 1986), where they show that the Hβ flux varies through the nebula. These errors could be minimized if new observations of HII regions are made in the positions observed by the IUE.

Regarding the comparison of our results with the solar abundances, Table 12, shows that the abundances are reduced by approximately the same amount for carbon, nitrogen and oxygen in the LMC; however, in the SMC this reduction is greater for the nitrogen abundance. These results are consistent with a scenario where oxygen is mainly due to primary production by massive stars, while C and N have an important contribution from intermediate mass stars; thus in the galaxies the O/H, C/O and N/O ratios are initially very low and increase with their subsequent chemical evolution. In Figures 6, 7 and 8 we present these ratios as a function of the total heavy elements abundance, Z, wich is given by the geometric mean of the Ne, S and Ar chemical abundances.

Table 13 shows an overall good agreement between our results and those of the literature. The only significant discrepancy is the abundance of nitrogen in the LMC, with a difference of 0.4 dex between our results and the literature. This could be because LMC HII regions have a large infrared flux due to a large amount of dust in this galaxy (van-Loon et al. 2008). For the SMC this difference is only < 0.1 dex.

For the SMC the difference in C/O between the multiple authors labeled as f, for F-K stars (Table 12), and (Garnett et al. 1995) (Table 10) is Δ=+0.34 dex, while that between these authors and our results is Δ=+0.19 dex. Garnett et al. used N88A to estimate C/O; the N88A observations show a large amount of dust: this is confirmed by our results. The dust produces an additional internal extinction for the ultraviolet carbon line, thus underestimating C/O. The biggest difference is observed for nitrogen with about Δ=+1.2 dex between red giant stars and HII regions, both for the LMC and SMC. This result is consistent with a transformation of C into N during the first dredge-up and subsequent mixing of this material in the most external layers of the atmosphere during the stellar evolution in the red giant branch (RGB).

TABLE 12

AVERAGE ABUNDANCES FOR DIFFERENT TYPES OF OBJECTS

HII	ϵ(He)	ϵ(C)	ϵ(N)	ϵ(O)	ϵ(Ne)	ϵ(S)	ϵ(Ar)	C/O	N/O	ϵ(Z)
LMC:										
HII[a]	10.93	8.03	7.37	8.33	7.73	6.82	5.97	-0.30	-0.96	6.84
PN (non-Type I)[b]	11.06	9.03	7.92	8.40	7.51	6.88	6.02	0.63	-0.48	6.80
PN (Type I)[b]	11.31	7.33	8.64	8.25	7.44	7.15	6.25	-0.92	0.39	6.95
FGK[c] Stars	—	8.04	8.60	8.40	—	—	—	-0.36	0.20	—
B Stars[d]	11.00	7.42	7.61	8.45	8.40	6.40	—	-1.03	-0.84	—
SNRs[e]	—	7.66	7.45	8.25	7.50	6.62	6.59	-0.59	-0.80	6.90
PN/HII	0.12	1.10	0.61	0.08	-0.32	0.06	0.08	—	—	—
Sun/HII	0.06	0.52	0.60	0.54	0.36	0.45	0.59	—	—	—
SMC:										
HII[a]	10.91	7.39	6.55	7.96	7.17	6.32	5.72	-0.57	-1.41	6.40
PN[b]	11.04	9.01	7.80	8.24	7.28	6.79	5.66	0.77	-0.44	6.57
F-K[f] Stars	—	7.68	7.76	8.06	—	—	—	-0.38	-0.30	—
B Stars[g]	—	7.65	7.12	8.32	—	—	—	-0.67	-1.20	—
SNRs[e]	—	—	6.88	7.93	6.89	6.45	—	—	-1.05	—
PN/HII	0.13	1.56	1.27	0.28	0.13	0.42	-0.07	—	—	—
Sun/HII	0.08	1.16	1.42	0.91	0.92	0.95	0.84	—	—	—
The Milky Way:										
Sun[h]	10.98	8.47	7.87	8.73	7.97	7.16	6.44	-0.26	-0.86	7.16
Orion[i]	10.99	8.52	7.73	8.73	8.05	7.22	6.62	-0.21	-1.00	7.27
M8[j]	11.01	8.69	7.72	8.51	7.81	6.94	6.52	—	—	7.09
M17[j]	10.97	8.77	7.62	8.52	7.74	7.01	6.39	—	—	7.05

[a]This work; [b] (Carlos-Reyes 1997); [c] (Russell & Bessell 1989), (Luck & Lambert 1992), (Spite et al. 1993), (Barbuy et al. 1994), (Hill et al. 1995); [d] (Rolleston et al. 1996); [e] (Russell & Dopita 1990); [f] (Russell & Bessell 1989), (Spite et al. 1989), (Luck & Lambert 1992), (Hill et al. 1997); [g] (Rolleston et al. 1993); [h] (Asplund et al. 2009); [i] (Esteban et al. 2004); [j] (García-Rojas et al. 2007).

TABLE 13

COMPARISON WITH RESULTS FROM THE LITERATURE

HII	ϵ(He)	ϵ(C)	ϵ(N)	ϵ(O)	ϵ(Ne)	ϵ(S)	ϵ(Ar)
LMC:							
This work	10.93	8.03	7.37	8.33	7.73	6.82	5.97
Literature	10.93	7.82	6.96	8.40	7.66	6.80	6.16
SMC:							
This work	10.91	7.39	6.55	7.96	7.17	6.32	5.72
Literature	10.92	7.26	6.49	8.05	7.24	6.44	5.85

On the other hand, thanks to our photoionization modelling, an important set of physical parameters can be determined, which are presented in Table 14. The first column shows the object name. In Columns 2 to 12 we present, successively, the luminosity of the ionizing source, the optical depth, the effective temperature of the central star; the external radius, the ionizing temperature, the density, the filling factor, the ionized mass, the reddening coefficient, the dust/gas ratio (relative to the local ISM) of the nebula, and the exponent for the radial distribution of the hydrogen density.

We have organized several values of the parameters as a function of the logarithm of their corresponding values; the luminosity and temperature of the central object were derived by assuming that the object is a single star with a given temperature. Certainly this is not the case in an HII region; however, the equivalent values are useful in the study of the basic parameters and the evolutionary status of the ionizing objects. From the set of 12 objects, 10 have ionizing temperatures between 41000 K and 56000 K, and luminosities above the zero-age main sequence (ZAMS). The most luminous case is N157 (30 Doradus Nebula), with a luminosity of about 10^4 times the ZAMS luminosity (Peimbert 2003). The most striking feature in the H-R (Hertzsprung-Russell) diagram is the location of two objects, N88A and N12B, below the ZAMS line (Figure 9). We interpret them as nebulae being ionized by evolved massive stars. We think it is not just by chance that these two nebulae have the largest dust/gas ratios and the highest extinctions.

6. CONCLUSIONS

In this work we have carried our a photoionization modeling for 11 HII regions of the MCs, six regions in the LMC and five in the SMC. A comprehensive modelling was done, employing ultraviolet,

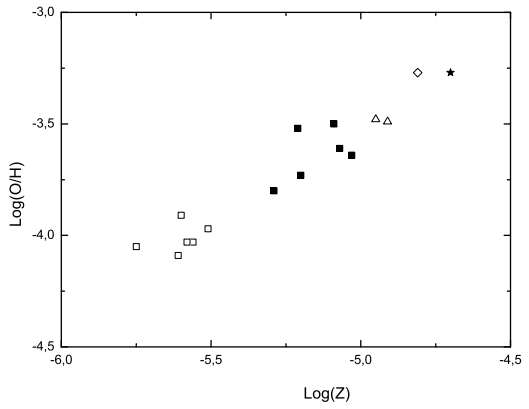

Fig. 6. Variation of O/H abundance ratio versus Z, in logarithm. Z is the geometric mean of abundances relatives to hydrogen for neon, sulphur and argon. The values represented with white square symbols correspond to HII regions in SMC, and the black square symbols to HII regions in LMC. These last data correspond to this work, whereas to literature correspond as follows: triangles correspond to HII regions in our galaxy, the rhombus corresponds to the Orion nebula, the asterisk corresponds to the solar abundance.

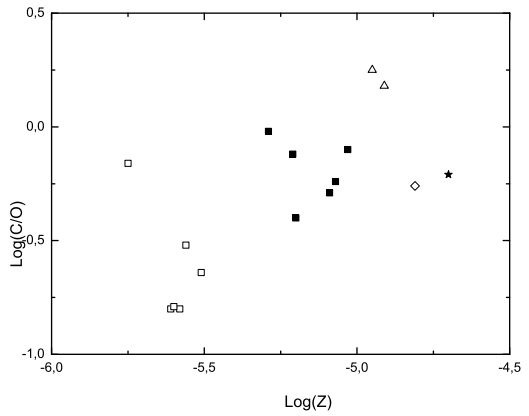

Fig. 7. Variation of C/O abundance ratio versus Z, in logarithm. Z is the geometric mean of abundances relatives to hydrogen for neon, sulphur and argon. The symbols correspond to the same objects from Figure 6.

optical and infrared data. The dust abundance in the MCs is not negligible, as can be inferred from the infrared flux observed by the IRAS satellite (Table 6), and in some cases the dust/gas ratio in the

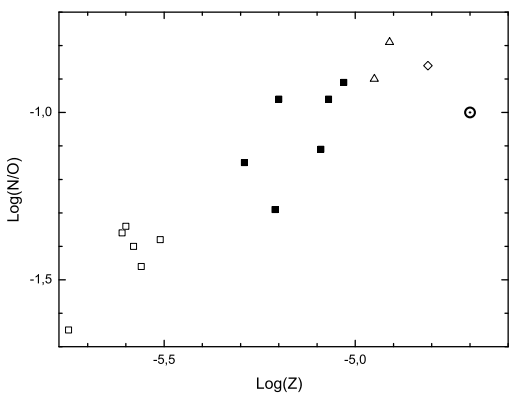

Fig. 8. Variation of the N/O abundance ratio versus Z in the logarithm. Z is the geometric mean of abundances relatives to hydrogen for neon, sulphur and argon. The symbols correspond to the same objects as in Figure 6 except that the circled dot corresponds to the solar abundance.

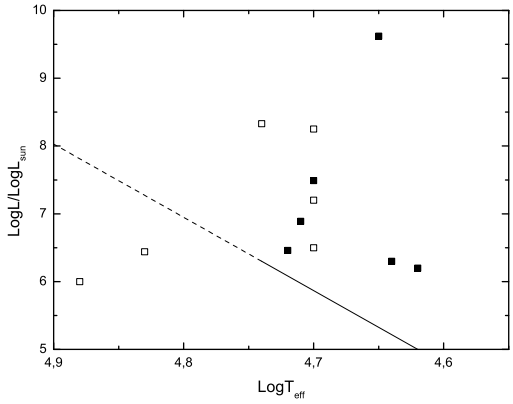

Fig. 9. HR Diagram of luminosity (normalized to the solar luminosity) versus effective temperature $T_{\rm eff}$, in the logarithm. The values represented with white squares correspond to HII regions in the SMC, and the black squares to HII regions in the LMC. The solid and dotted lines represent the ZAMS.

MCs is higher (by a factor of 2 or 4) than the corresponding one for our galaxy's ISM.

The carbon abundances for HII regions were obtained for our sample (Table 11); this result is important because it establishes more precisely the current value of this abundance in the MCs. The chemical abundances of helium, carbon and oxygen are, in general, and within the errors, in agreement with

TABLE 14

PHYSICAL PARAMETERS FOR HII REGIONS IN THE MCS

HII	$\log L$ ($L_\odot$)	$\log T_{\rm eff}$ (K)	$\log R$ (cm)	$\log T_{\rm e}$ (K)	$\log N_{\rm e}$ ($\rm cm^{-3}$)	$\log\tau$	$\log\epsilon$	$\log M_{\rm ion}$ ($M_\odot$)	c	dust/gas	γ
LMC:											
N4A	6.30	4.64	19.37	3.97	2.34	-0.23	-1.70	2.44	0.25	—	-0.02
N11A	6.20	4.62	18.82	3.97	2.80	-0.22	-1.15	1.79	0.22	—	0.00
N79A	7.49	4.70	20.01	3.98	2.90	-0.40	-3.52	3.07	0.35	—	-0.11
N157	9.62	4.65	20.84	4.03	2.65	-0.91	-4.00	4.84	0.44	—	-0.04
N159	6.89	4.71	20.04	4.04	1.84	0.62	-1.52	4.20	0.47	0.8	-0.56
N160A	6.46	4.72	19.47	3.96	2.34	0.78	-1.00	3.44	0.15	—	-0.11
SMC:											
N12B	6.44	4.83	19.84	4.13	2.31	-0.14	-2.52	2.95	0.20	2.3	0.00
N66A	8.33	4.74	20.52	4.14	2.48	-0.82	-3.70	4.01	0.18	0.7	-0.12
N66NW	8.25	4.70	20.53	4.11	2.45	-0.82	-3.82	3.92	0.09	0.9	-0.32
N81	7.20	4.70	20.02	4.10	2.30	-1.08	-1.00	2.73	0.07	0.6	-0.13
N83A	6.50	4.70	19.93	4.07	1.99	-0.05	-2.30	3.30	0.18	—	-0.69
N88	6.00	4.88	19.67	4.13	1.80	1.66	-1.09	3.45	0.49	4.5	-0.44

the literature. The largest discrepancy is found for nitrogen in the LMC, our value being 0.4 dex higher than that in the literature. However, the abundance of argon in LMC is almost 0.2 dex lower in this work; this result should be taken with caution because we only have two objects where the argon line was observed. For the SMC HII regions, the discrepancy is less than 0.1 dex for all chemical abundances.

When compared with the MCs young stars (B stars), the observed abundances of carbon and oxygen in HII regions are in agreement. The strong nitrogen deficiency observed in HII regions is in agreement with the results for FGK supergiants (Table 12). Additionally, the abundance of C + N is larger by a factor of three in FGK supergiants compared to the HII regions. However, the C/O ratio of FGK supergiants in the LMC is quite similar to that of HII regions. Finally, the dispersion observed in the chemical abundances of HII regions in the MCs suggests to us that the gas is not well mixed.

Rafael E. Carlos Reyes thanks the Brazilian entity CNPq (The National Council for Scientific and Technological Development) for its support through contract 381314/97-9. Likewise, F. Elizalde thanks INPE, where he was working during the development of the present research; he would like to clarify that he is not currently affiliated to INPE.

REFERENCES

Aller, L. H., Ross, J. E., Keyes, C. D., & Czyzak, S. J. 1979. S. J. Astroph. and Space Sc. 64, 347

Asplund, M., Grevesse, N., Sauval, A. J., & Scott, P. 2009, ARA&A, 47, 481

Barbuy, B., de Freitas Pacheco, J. A., & Castro, S. 1994. A&A, 283, 32

Caplan, J., & Deharveng, L. 1985. A&A SS, 62, 63

Caplan, J., Taisheng, Y., Deharveng, L., Turtle, A. J., & Kennicut, R. C. 1996. A&A, 307, 403

Carlos-Reyes, R. E. 1997. Parâmetros Físicos e Químicos de Nebulosas Planetárias nas Nuvens de Magalhães. PhD thesis, Instituto Astronômico e Geofísico da Universidade de São Paulo, Brazil

Davis, R. D., Elliott, K. H., & Meaburn, F. 1976. Mem. R. Astr. Soc., 81, 89

Dufour, R. J. 1984. In: IAU Symp No. 108, Eds S. van den Bergh & K. S. de Boer, 353

Dufour, R. J., Elliott, K. H., & Meaburn. 1975. ApJ, 195, 315

Dufour, R. J., & Harlow. 1977. W. V. ApJ, 216, 706

Dufour, R. J., Shields, G. A., & Talbot, R. J. 1982. ApJ, 252,461

Elizalde, F. 1997. Diagnóstico automático de nebulosas astrofísicas. PhD thesis, Instituto de Pesquisas Espaciais, São José dos Campos, São Paulo, Brazil

Esteban, C., Peimbert, M., García-Rojas, J., Ruiz, M. T., Peimbert, A., & Rodríguez, M. 2004. MNRAS 355, Issue 1, 229

Ferland, G. J. 2004. Hazy: A brief introduction to Cloudy 96.00. University of Kentucky, Department of Physics and Astronomy, Kentucky, USA

García-Rojas, J., Esteban, C., Peimbert, A., & Rodríguez, M., Peimbert, M., & Ruiz, M. T. 2007. RMxAA, 43, 3

Garhart, M. P., & Nichols, J. S. 1995. IUE Newsletter No. 55

Garnett, D. R., Skillman, E. D., Dufour, R. J., Peimbert, M., Torres-Peimbert, S., Terlevich, R.,and Terlevich, E., & Shields, G. A. 1995. ApJ, 443, 64

Hamuy, M., Suntzeff, Heathcote, S. R., N. B., Walker, A. R., Gigoux, P., & Phillips, M. M. 1992. PASP,

104:677:533
Hamuy, M., Walker, A. R., Suntzeff, N. B., Gigoux, P., Heathcote, S. R., & Phillips, M. M. 1994. PASP, 106:700:566
Henize, K. G. 1956. ApJS, 2, 315
Heydari-Malayeri, M., & Lecavelier des Etangs, A. 1994. A&A, 291, 960
Heydari-Malayeri, M., & Testor, G. 1982. A&A, 111, L11
_____. 1985. A&A, 144, 98
_____. 1986. A&A, 162, 180,
Heydari-Malayeri, M., Le Bertre, T., & Magain, P. 1988. A&A, 195, 230
Hill, V., Andrievsky, S., & Spite, M. 1995. A&A, 293, 347
Hill, V., B. Barbuy, and M. Spite. 1997. A&A, 323, 461
Jablonski, F. 1996. *Laboratorio Nacional de Astrofísica*, CNPq, Internal Report
Kajino, T., Kusakabe, M., Baha Balantekin, A., Mathews, G. J. &, Cheoun, M. K. 2012. In: XII International Symposium on Nuclei in the Cosmos, 353
Kennicutt, R. C. & P. W. Hodge. 1986. Ap.J. 306, 130
Kurt, C. M., Dufour, R. J., Garnett, D. R., Skillman, E. D., Mathis, J. S., Peimbert, M., Torres-Peimbert, S., & Walter, D. K. 1995. RMxAA, 3, 223
Leisy, P., & Dennefeld, M. 2006. A&A, 456, 451
Luck, R. E., & Lambert, D. L. 1992. ApJS, 79, 303
Mathis, J. S. 1990. Ann. Rev. Astron. Astrophys., 28, 37
Mathis, J. S., Chu, Y. H., & Peterson, D. E. 1985. ApJ, 292, 155
Mowlavi, N. 2001. ApSSc Library, 264, 287
Olive, K. A., & Steigman, G. 1995. Ap. J. S., 97, 49
Osterbrock, D. E., & Ferland, G. J. 2005. Astrophysics of Gaseous Nebulae and Active Galactic Nuclei. University Science Books, 2nd edition, USA
Pagel, B. E. J., Edmunds, M. G., Fosbury, R. A. E., & Webster, B. L. 1978. MNRAS, 184, 569
Pei, Y. C. 1992. ApJ 395, 130
Peimbert, A. 2003. ApJ, 584, 735-750
Peimbert, M., & Torres-Peimbert, S. 1974. ApJ, 193, 327
_____. 1976. ApJ, 203, 581
Peimbert, M., Torres-Peimbert, S., & Dufour, R. J. 1993. ApJ, 418, 760
Peimbert, M., Luridiana, V., & Peimbert, A. 2007. ApJ, 666, 636
Peters, T., Banerjee, R., Klessen, R. S., Mac Low, M-M., Galván-Madrid, R., & Keto, E. R. 2010. ApJ, 711, 1017
Pettini, M. 2004. in Cosmochemistry: The Melting Pot of the Elements 257-294. Eds: C. Esteban, R. J. García López, A. Herrero & F. Sánchez, Cambridge Contemporary Astrophysics, UK
Pottasch, S. R. 1984. Planetary Nebulae. Reidel, Dordrecht, Netherlands
Press, W. H., Teukolsky, S. A., Vetterling, W. T., & Flannery, B. P. 2007. Numerical Recipes: The Art of Scientific Computing. Cambridge University Press, 3rd edition, New York, USA
Rocca-Volmerange, B., Prevot, L., Prevot-Burnichon, M. L., Ferlet, R., & Lequeux, J. 1981. A&A, 99, L5
Rolleston, W. R. J., Dufton, P. L., Fitzsimmons, A., Howarth, I.D., & Irwin, M. J. 1993. A&A, 277, 10
Rolleston, W. R. J., Brown, P. J. F., Dufton, P. L., & Howarth, I. D. 1996. A&A, 315, 95
Rolleston, W. R. J., Venn, K., Tolstoy, E., & Dufton, P. L. 2003. A&A, 400, 21
Russell, S. C., & Bessell, M. S. 1989. ApJS, 70, 865
Russell, S. C., & Dopita, M. A. 1990. ApJS, 74, 93
Schwering, P. B. W., & Israel, F. P. 1990. Atlas and Catalogue of Infrared Sources in the Magellanic Clouds. Kluwer Academic Publishers, Dordrecht, Boston/London, UK
Seaton, D. K. 1979, MNRAS, 187:4:785
Smecker-Hane, T. A., Cole, A. A., Gallagher III, J. S., & Stetson, P. B. 2002. ApJ, 566, 239
Sofia, U. J., Gordon, K. D., Clayton, G. C., Misselt, K., Wolff, M. J., Cox, N. L. J., & Ehrenfreund, P. 2006. ApJ, 636:2:753
Spite, F., Barbuy, B., & Spite, M. 1993. A&A, 272, 116
Spite, M., Spite, F., Barbuy, B. 1989. A&A, 222, 35
Stasińska, G. 2012. Oxygen in the Universe. EAS, EDP Sciences, Vol. 54, pp. 255, France
Steigman, G. 2004. in Cosmochemistry: The Melting Pot of the Elements 1-30. Eds: C. Esteban, R. J. García López, A. Herrero & F. Sánchez, Cambridge Contemporary Astrophysics, UK
Testor, G. & Pakull, M. 1985. A&A, 145, 170
van Loon, J. Th., Cohen, M., Oliveira, J. M., Matsuura, M., McDonald, I., Sloan, G. C., Wood, P. R., & Zijlstra, A. A. 2008. A&A, 487:3:1055
Vermeij, R. & van der Hulst, J. M.2002. A&A, 391, 1081

Rafael Edgardo Carlos Reyes: Facultad de Ciencias Físicas, Universidad Nacional Mayor de San Marcos (UNMSM), Calle Germán Amézaga N^o 375, Lima 1, Perú (raedcare@hotmail.com).
Flavio Elizalde: Instituto Nacional de Pesquisas Espaciais, Divisão de Astrofísica - DAS/INPE, São Paulo, Brazil.
Jorge Meléndez and João Steiner: Universidade de São Paulo, IAG/USP, São Paulo, Brazil.
Felipe Américo Reyes Navarro: Universidad Nacional Mayor de San Marcos, UNMSM, Lima, Perú.